COMPUTATIONAL BEAM DYNAMICS FOR SNS COMMISSIONING AND OPERATION *

J. Holmes#, S. Cousineau, V. Danilov, S. Henderson, D.-O. Jeon,
M. Plum, A. Shishlo, Y. Zhang, ORNL, Oak Ridge, TN 37831, U.S.A.
D. Bartkoski, University of Tennessee, Knoxville, TN, 37996, U.S.A.

Abstract

The computational approach is providing essential guidance and analysis for the commissioning and operation of SNS. Computational models are becoming sufficiently realistic that it is now possible to study detailed beam dynamics issues quantitatively. Because of the variety of phenomena considered, the most successful models are being developed with modularity and flexibility of use. Increasingly, we are seeing that the biggest challenge in performing successful analyses is that of knowing and describing the machine and beam state accurately. Even so, successful benchmarks with both theoretical predictions and experimental results are leading to increased confidence in the capability of these models. With this confidence, computer codes are being employed in a predictive manner to guide the machine operations. We will illustrate these points with various examples taken from the SNS linac and ring.

INTRODUCTION

The Spallation Neutron Source (SNS) is on track to become the world's most powerful pulsed neutron source. At full operating parameters, it will deliver 1.5×10^{14} protons at 1.0 GeV to a liquid mercury target 60 times every second. The power on target will be 1.44 MW. The SNS accelerator consists of a negative ion source followed by a full energy linac and an accumulator ring. The linac consists of several stages, with acceleration to 186 MeV at room temperature and from 186 MeV to 1 GeV in the world's first superconducting RF proton linac (SCL). The SCL contains two sections: a medium beta (MB) section of eleven cryomodules with three β=0.61 cavities per cryomodule, and a high beta (HB) section of twelve cryomodules with four β=0.81 cavities per cryomodule. The MB section accelerates the H^- ions from 186 MeV to 387 MeV and the HB section accelerates from 387 MeV to 1 GeV. Because of the intense beam, SNS must operate with unprecedented low beam losses: 1.0×10^{-4} uncontrolled beam loss and 1.0×10^{-3} total beam loss.

The commissioning of SNS was carried out in stages, starting with the Front End in late 2002 and finishing with the target early this summer (2006). It is notable that a peak beam energy of 952 MeV and a peak target pulse of 5×10^{13} protons have been achieved. Although all of the commissioning milestones were met, there are major hurdles to cross between now and full operation. At present, beam losses restrict operation to low power. However, we are pursuing an aggressive schedule: by April, 2007, we intend to be operating at 100 kW, and full power operation is scheduled for October, 2009.

There are numerous applications of computing to SNS commissioning and operation. Obviously, there is almost nothing about SNS that isn't intimately connected to computers in some way. In the area of accelerator physics, there are two major approaches: 1) on-line software applications used in the control room to operate, diagnose, and correct the machine, and 2) simulations used to study design and operational issues and to benchmark and understand experimental results. In terms of physics models, the on-line applications are simple and fast so that they can be used to guide real time machine operation. They also tend to be directly linked to the accelerator diagnostics and control system. Simulation codes typically have much more complicated physics models, are more time intensive to run, and are not involved in direct accelerator operation. Simulation codes are used to study physics issues relating to machine design and operation as well as to analyze and understand experimental data. It is worth pointing out that the diversity and complexity of demands on both on-line and simulation models strongly drive the development of modular, object-oriented codes with flexible user interfaces and problem definition. We will confine the present discussion to beam dynamic simulations that address operational issues or examine experimental results. We omit the wealth of on-line control room software developed for SNS.

In particular, we will present a number of examples of the use of simulation codes to analyze SNS data and issues. For conducting simulations in the SNS linac, we use the codes Parmila [1], Impact [2], and Trace3D [3]. We will show two examples of their use: 1) the analysis of beam halo in the warm linac, and 2) SCL fault studies. For the study of issues in the accumulator ring, we use the ORBIT Code [4] with the lattice setup supported by MAD [5]. ORBIT contains a comprehensive suite of physics and diagnostic models, and it has been applied to a wide range of SNS design, commissioning, and operation issues. We present here a number of examples of these ORBIT simulations: 1) magnet errors and correction, 2) measurement of tunes, 3) excited H^0 decay and losses after stripping, 4) transverse stability limits due to the extraction kicker impedance, and 5) an electron cloud stability estimate. Following these examples we present some concluding thoughts.

* ORNL/SNS is managed by UT-Battelle, LLC, for the U.S. Department of Energy under contract DE-AC05-00OR22725
#jzh@ornl.gov

BEAM HALO SIMULATIONS

One of the key issues confronted during commissioning of the warm linac was that of matching the beam from the RFQ into the DTL. This is carried out in the MEBT, where the beam is longitudinally bunched and transversely focused. The transverse matching is carried out primarily through the use of the last four quadrupoles in the MEBT. Their strengths were optimized with the use of beam profiles taken by wire scanners at various locations throughout the warm linac. The resulting experimentally obtained beam profiles were well described by Gaussian distributions from the central peak down to about the 5% level. Below this, the profiles were broader, showing a significant halo component. By varying the strengths of the four matching quadrupole magnets, the amount and extent of beam halo was observed to vary.

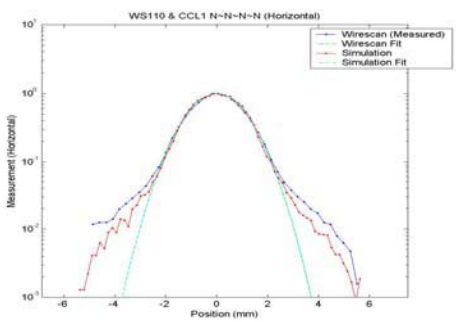

Figure 1: Typical result for comparison of experimental and simulated beam profiles in the warm linac.

It was decided to simulate the beam transport from the RFQ through the MEBT and the warm linac for comparison with the experimental results [6]. The simulations were conducted using Parmila. The settings of the MEBT quadrupoles were varied as in the experiments for three initial distributions: 1) a reference distribution based on earlier measurements of the beam at the exit of the RFQ, 2) a 6D Gaussian distribution, and 3) a waterbag distribution. All three distributions were specified to have the rms emittances resulting from those earlier measurements. For all three initial distributions, the results showed excellent systematic agreement between simulation and experiment for the central beam core. With respect to halo, both experimental and simulated results (with all three initial distributions) varied with location and with MEBT quadrupole strengths, and all tended to decrease through the CCL. However, detailed systematic agreement between calculated and measured beam halo (below a few percent of peak), or between simulated halo from different initial distributions, was not obtained. Figure 1 shows a typical comparison between measured and calculated results with good agreement in the beam cores and detailed differences in beam halo. Based on our experience, we believe the main uncertainties were the lack of detailed knowledge of the initial beam distribution from the RFQ, of the values of the lattice functions, and of the precise phase advances through the linac at the time of the measurements. The accurate computation of small sensitive quantities requires such information.

SCL FAULT SIMULATIONS

SNS features the world's first superconducting proton linac. Beam losses in the SCL could have serious consequences, such as quenching the cavities, generating arcs at the power couplers, or severely activating or damaging components. The most dangerous faults in the SCL are those with the most localized beam losses. Because of the serious consequences of potential SCL beam losses, a number of simulations of SCL beam faults have been conducted. This work was used to provide guidance in the determination of Machine Protection System (MPS) time response requirements for the termination of beam. Two types of simulation were considered. A study of various combinations of magnet failures was conducted using Parmila. This study found the following results: 1) the beam will survive single quadrupole or steering magnet faults; 2) if a chain of several quadrupoles fails, 90% of beam may be lost over two cryomodules (~10% in each cavity in that range); 3) if all SCL quadrupole strengths increase or decrease by 50%, beam losses will be spread over the SCL with maximum localized losses ~50% in individual cavities. When the time constants of the quadrupoles and steerers are considered, disastrous beam loss in the SCL due to the worst quadrupole faults can be prevented if MPS response is no more than a few tens of microseconds. A second, and more dangerous, fault scenario is that of RF cavity failures, which we studied using Impact. We examined two major scenarios: 1) failure of and sensitivity to the first MB cavity, cryomodule, or modulator, and 2) failure of and sensitivity to a HB cavity, cryomodule, or modulator. We found that rapid beam blow up may be triggered if the amplitude of the first medium beta cavity is reduced 40% or the phase is shifted 20°. We also found that, if the amplitude of the first modulator (four cryomodules, twelve cavities) is reduced ~5%, catastrophic beam losses in the SCL will occur. This is a challenge to the LLRF feed-forward system as the influence of beam loading on the cavity amplitude is more than 5%, and it is known that cavity phase is also affected by the beam loading. In general, the farther upstream in the SCL a fault occurs, the greater is the danger of catastrophic beam loss. These studies suggest that MPS response must be as fast as practically possible, ~10 μs for safe commissioning.

ERROR CORRECTION IN THE RING

We have carried out a thorough study of the effects and correction of misalignments and field strength errors in the SNS ring [7]. ORBIT was the primary tool used in this study. In addition to the usual beam dynamics models in ORBIT, these studies rely on ORBIT's error models, BPM and dipole corrector models, orbit correction routine, and aperture and collimation models.

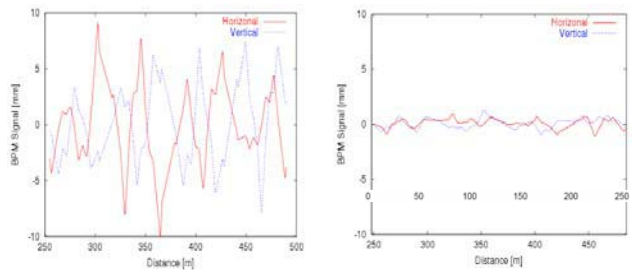

Figure 2: BPM signals around the ring for uncorrected and corrected worst case errors.

Various errors were considered individually and also in conjunction with other errors via random generation using uniform distributions. The errors included displacements and rotations of all magnets as well as errors in the field strengths. The magnitude of the errors was always taken to be greater than or equal to the SNS tolerance. The closed orbit was corrected by adjusting dipole corrector strengths to minimize BPM signals. Two methods were employed, least square minimization and the 3-bump method, with nearly identical results. BPM signal errors were also assumed, and were generated randomly according to a Gaussian distribution with σ_{rms}=1.0 mm, σ_{cutoff}=2.0 mm. Quadrupole field strength errors were corrected using phase advance information calculated using MAD. For the purpose of field error correction, phase advances at specific BPMs were assumed to be obtainable to within ±3.6° with a uniform distribution. Quadrupole and dipole roll errors were not corrected because they were found to have no significant effect on the beam. In all error correction studies, attention was paid to the identity of families of magnets sharing common power supplies. In addition to studying the effects of individual errors, cases were considered with all errors simultaneously activated. Without correction, the worst case beam loss is 49%, with losses starting before 400 turns of the 1060 turn injection. With orbit and phase correction, assuming no BPM errors, losses are less than 10^{-4}. Even with random BPM signal uncertainties, total losses are still only 1.7×10^{-4}. The BPM signals around the ring for the uncorrected and corrected beams are shown in Fig. 2 for this case. These results have been found to hold in general for many cases considered and have provided confidence in SNS error correction capabilities and guidance to the development of the on-line error correction models.

TUNE MEASUREMENT

Various techniques for tune measurement in the SNS ring have been studied using ORBIT [7]. In SNS, BPMs are used to measure both the betatron tune and phase advance around the ring. The BPMs have both base-band (a few MHz) and narrow-band (402.5 MHz, the injected linac bunch frequency) capability. Because the 402.5 MHz band has higher resolution at low intensity, we assessed the lifetime of the 402.5 MHz structure in the ring. This was done using two models: an analytic model and ORBIT simulations. For the analytic model, we considered an ellipsoidal beam with uniform density in a transverse uniform focusing channel and with free expansion in the longitudinal direction. For the initial condition, we used the expected transverse emittances, longitudinal, and energy distributions at the end of the SCL. This model predicts that, for these parameters, essentially all space charge effects occur in approximately the first 250 meters, after which the bunch expansion proceeds based on the energy spread developed during that time. According to this analytic model, the linac microbunch size reaches the inter-bunch spacing in about 9 turns. The ORBIT simulation model tracks the distribution of a single linac microbunch through the ring. Initial conditions were taken to be the expected transverse emittances, longitudinal, and energy distributions at the injection foil. Calculations were carried out using both the full 3D space charge model and, for comparison, the simple longitudinal space charge model. The ORBIT simulations show decoherence of the 402.5 MHz signal in about 5 turns (Fig. 3), which is in fair agreement with the analytic model prediction. The implication of these calculations is that, with 5-10 turns of data, single shot narrow-band BPM signals can be used for tune calculations, but we should expect errors due to the low number of turns. It should be mentioned that ORBIT has been benchmarked against experimental single turn injection data from PSR, which has a 201 MHz linac signature. The data shows decoherence of the 201 MHz structure in about 30 turns followed by the reappearance of the structure about 1000 turns (one half synchrotron period) later. ORBIT simulations show the same longitudinal dynamics, including the 30 turn decoherence and the reappearance 1000 turns later.

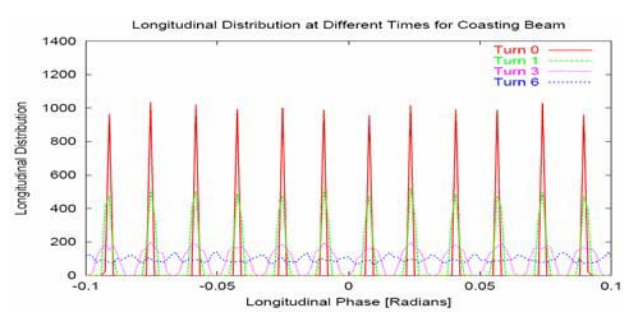

Figure 3: Longitudinal current distribution at 0, 1, 3, and 6 turns.

Single turn injection BPM data were simulated with ORBIT, post-processed, and then fit with a CERN Lib fitting program to obtain the horizontal betatron tune. The bare tune was known to be $\nu_x = 6.23$. Both narrow band (402.5 MHz) and base band signals were used. As discussed above, narrow band data are available for about 5-10 turns. For natural chromaticity, base band data is available for about 50 turns before it decoheres. Random BPM errors of 1.0 mm were assumed for narrow band fitting and 2.0 mm for the less sensitive base band fitting. Results for the fractional tunes were the following: For

the narrow band fit we obtained $\nu_x = 0.2324 \pm 0.0044$, while the base band fit gave $\nu_x = 0.2325 \pm 0.00065$.

ORBIT was also used to study tune calculation due to kicking an accumulated beam. The chosen scenario was to accumulate a beam for 50 turns, then allow it coast up to 300 turns, at which time it is given a kick of 1.5 mradians. The kicked beam was then followed until decoherence, approximately 50 more turns, and the BPM signals analyzed to obtain the fractional tune. In this case, a BPM error of 1.0 mm was assumed for fitting, which is smaller than for the single-shot measurement because of the higher beam intensity. In this case the fitted tune was found to be $\nu_x = 0.2381 \pm 0.00034$, as shown in Fig. 4. Figure 4 also shows that, when the sextupoles are used to zero the chromaticity, the signal lasts much longer, thus allowing very precise tune calculations. In the example shown here, the precision of the zero chromaticity measurement is about an order of magnitude better than the case with chromaticity. The base-band methods have been implemented in the on-line models at SNS.

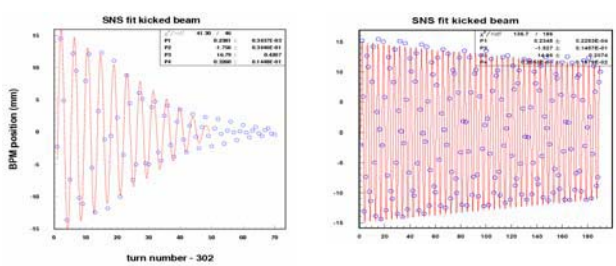

Figure 4: BPM signal and fit for kicked beam with natural (left) and corrected (right) chromaticity.

TRANSVERSE STABILITY OF THE RING

Because the 248 meter SNS ring will ultimately operate at the extremely high beam intensity of 1.5×10^{14} 1-GeV protons, transverse instabilities are a concern. Accordingly, we conducted a broad study of transverse stability in SNS [8]. We began by studying analytic coasting beam models [9,10] in the SNS parameter regime and by applying the results of these studies to benchmark the transverse stability model in the ORBIT code. We varied all relevant parameters, including analytically solvable (for benchmark purposes) energy distributions, chromaticity, and space charge. We used KV transverse beam distributions in these studies. With this confirmation of the accuracy of ORBIT, we then carried out stability calculations for realistic bunched beams obtained during injection. For comparison with the coasting beam results, these latter calculations were first carried out with single harmonic impedances. Finally, transverse stability was calculated for the full injection process using the measured extraction kicker impedance [11], which is dominant in the ring.

As an extension of the coasting beam calculations, we constructed "SNS coasting beams" as follows: Using ORBIT, we injected a beam of 1.5×10^{14} protons over 1060 turns into the SNS ring. The dynamics included transverse painting, symplectic tracking, space charge, the ring RF focusing, and the longitudinal and transverse impedances from the extraction kickers, which dominate the ring. The peak distribution at the longitudinal center of the bunch was used to generate a coasting beam of the same shape and intensity. The resulting energy distribution was fit by simple functions that could be used analytically to provide stability diagrams. The distribution was well represented by the sum of rectangular and Gaussian contributions, as shown in Fig. 5. The bunch factor for this case in the ORBIT injection simulation was 0.4, so we used $N = 3.75\times10^{14}$ protons in the coasting beam simulations here.

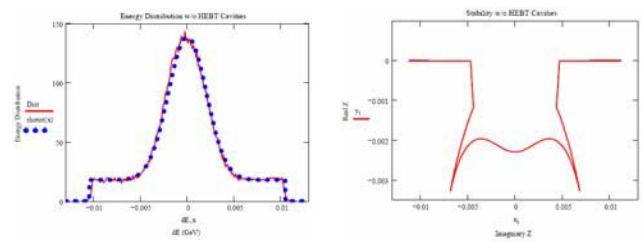

Figure 5: Left) energy distribution of "SNS coasting beam". Red curve is from simulation and blue curve is fit using Gaussian plus rectangular distribution. Right) stability diagram for given energy distribution.

The stability diagram resulting from the "SNS Coasting beam" is shown in Fig. 5. The axes correspond to imaginary (horizontal) and to real (vertical) impedances, respectively. The stability diagram is valid for different values of phase slip factor, chromaticity, intensity, and mode number, but the scales depend on all these factors [8]. Taking that into account, the analytic instability thresholds from the stability diagram in Fig. 5 have been compared with computational ORBIT results for a real impedance with $n = 10$ for several cases. The results show that ORBIT is in good agreement with the analytic predictions, as shown in Table 1. The cases are as follows: 1) linear tracking, no space charge; 2) symplectic tracking, corrected chromaticity, no space charge; 3) symplectic tracking, natural chromaticity, no space charge; 4) linear tracking, with space charge; and 5) bunched beam, natural chromaticity, no space charge.

Table 1. SNS Coasting Beam Stability Results

Case	Analytic Threshold (kΩ/m)	ORBIT Stable (kΩ/m)	ORBIT Unstable (kΩ/m)
1	25.6	25	30
2	25.6	30	40
3	242	200	300
4	0	0	10
5		800	1000

Comparing Cases 3 and 5 in Table 1 shows that bunched beams appear significantly more stable than do coasting beams. Because SNS will operate with bunched beams, we carried out several bunched beam simulations

with ORBIT. These were done for 1060 turn injection of 1.5×10^{14} protons. The calculations included transverse injection painting, the ring RF longitudinal focusing, the extraction kicker longitudinal and transverse impedances, and variations on the single particle transport and presence of space charge forces. In all cases, thresholds were obtained in terms of impedances by multiplying the extraction kicker impedance by constant factors. The results are shown in Table 2. The cases are as follows: 1) linear tracking, no space charge; 2) symplectic tracking, corrected chromaticity, no space charge; 3) symplectic tracking, natural chromaticity, no space charge; 4) linear tracking, with space charge; 5) symplectic tracking, corrected chromaticity, with space charge; and 6) symplectic tracking, natural chromaticity, no space charge. The results of Cases 3 and 6 show, as in the coasting beam calculations, that chromaticity provides significant stabilization. We also see from Cases 1 and 2 that, if space charge is neglected, SNS at zero chromaticity is predicted to be unstable at the extraction kicker impedance. The relevant rows are Cases 4-6, which are the same as Cases 1-3, respectively, except for the inclusion of space charge. Unlike the coasting beam case in Table 1, for which space charge is strongly destabilizing, the effect of space charge on the SNS bunched beam is stabilizing to the zero chromaticity case and very mildly destabilizing at natural chromaticity. Most important, we see that SNS should be stable with at least a factor of 2 to spare over the extraction kicker impedance. We have recently experimentally induced a coasting beam instability in SNS with the frequency signature of the extraction kicker impedance, but have not yet had time to carry out its simulation.

Table 2. SNS Bunched Beam Stability Results

Case	ORBIT Stable ×Z	ORBIT Unstable ×Z
1	0.5	0.6
2	0.6	0.8
3	5	7
4	1.5	2
5	2	3
6	3	4

ELECTRON CLOUD MODULE

The instabilities caused by coupled electron-proton oscillations can limit the performance of intense proton storage rings. The electron-cloud effect (ECE) shows itself very clearly in the Proton Storage Ring (PSR) at Los Alamos National Laboratory [12]. Due to similarities between PSR and SNS, dedicated electron cloud studies and countermeasures have been considered from the early stages of the SNS project. Countermeasures include low secondary electron emission titanium nitride (TiN) beam pipe coating, an electron collector near the stripping foil, and reserved space for solenoid magnets to reduce electron buildup in high loss regions.

The ORBIT code has been used to study the stability of the beam in the SNS ring with respect to electron cloud effects [13]. ORBIT's electron cloud model has been applied to analytic benchmark studies, to PSR, and to SNS. It has the following properties: 1) the model is self-consistent in that both the ambient electrons, modeled as macroparticles, and the proton beam are tracked under their own and each other's space charge forces and external forces; 2) The effects of electron generation and wall interactions have been incorporated using the models of Pivi and Furman [14].

Our computations consist of two stages: electron cloud development simulations and proton bunch stability studies in the presence of ECE.

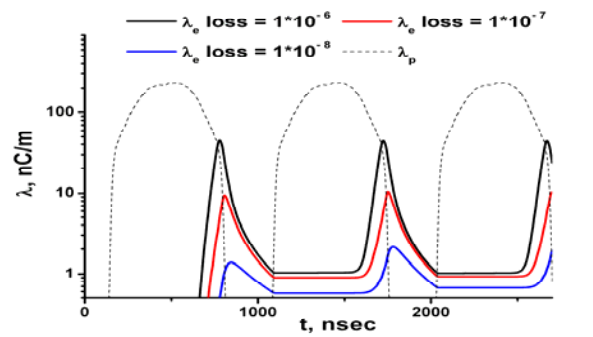

Figure 6: Simulated electron and proton bunch densities during the first SNS bunch passages for different proton loss rates per turn, for a magnetic field-free region.

We first studied the electron cloud formation. One electron cloud node was placed in the ring lattice at a position with average values of the transverse beta-functions. The longitudinal positions of the protons were frozen, and the bunch density was the same for each turn. The electron densities are shown as functions of time in Fig. 6. The simulations were performed for different proton losses in the ring. The design value of proton loss for SNS is 0.1% of the beam intensity during the whole accumulation period of 1060 turns, which gives about 10^{-6} probability of loss per turn per proton. These losses will occur mostly in the ring collimator. The smaller values of the loss coefficient may be appropriate in other parts of the SNS ring. The variation of losses over two orders of magnitude leads to only a factor of two difference in the electron densities. The plateau, rather than peak, values are most relevant for stability analysis. Smaller loss rates give more stable proton beams. Simulations of e-cloud formation have been performed for dipole magnet regions also. They give smaller peaks and plateau values than those for field-free places.

During the proton beam instability simulations two variants of tracking were compared. In the first, the longitudinal positions of the macro-particles representing the bunch were frozen. This was accomplished by setting their energies to the design energy of the beam. In this case, there is no Landau damping and an instability of the transverse motion of the proton beam is found (Fig. 7). Figure 7 shows the average Fourier spectrum amplitudes

of the horizontal motion of the beam center as a function of the turn number. The Fourier amplitudes were averaged over the peak 116-120 MHz frequency region. The results demonstrate a clear growth, and as hoped, it is slower than is observed for PSR.

For the second case of simulations the actual energy spread of the macro-protons in the bunch was used. The value of the spread corresponds to 30% of the nominal voltage in the rf-bunchers of the SNS ring. The damping caused by this spread completely suppresses any instability in the transverse beam motion (Fig. 7). These calculations indicate that SNS should be stable with respect to ECE. An EC instability has been experimentally induced in the SNS ring at an intensity 2.5×10^{13} protons for a coasting beam with no chopping [15]. These results can not be compared with the present simulations because of the lack of longitudinal bunching in the experiment. This instability and its simulation will be subject of further investigations.

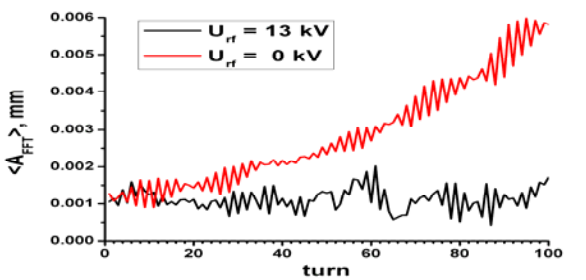

Figure 7: Average Fourier amplitudes of the horizontal oscillations of the center of the proton bunch in the SNS ring.

DISCUSSION

Much of the computing required to support SNS commissioning and operation does not require ultra-high performance. Exceptions include transverse instability studies, which require a 3D description of space charge, and electron cloud studies, when the proton beam response is included. Most important is to incorporate a broad range of physics models to describe the many issues encountered. The variety and sophistication of our models has increased considerably with time. Because of the need for a broad range of models to address the great diversity of phenomena encountered, it is important to develop modular software and a convenient and flexible user interface. The main source of inaccuracy/error in simulating hypothetical or measured phenomena is most likely our lack of complete detailed knowledge of the actual operating conditions.

ACKNOWLEDGEMENT

This research used resources of the National Energy Research Scientific Computing Center (NERSC), which is supported by the Office of Science of the U.S. Department of Energy under Contract No. DE-AC03-76SF00098.

REFERENCES

[1] H. Takeda, "PARMILA", LA-UR-98-4478 (2000), LANL.

[2] J. Qiang and R.D. Ryne, "IMPACT", (2004), LBNL.

[3] K. Crandall and D. Rusthoi, "Trace3D Manual (3rd ed.)", LA-UR-97-886 (1997), LANL.

[4] J.A. Holmes, S. Cousineau, V.V. Danilov, J. Galambos, A. Shishlo, W. Chou, L. Michelotti, F. Ostiguy, and J. Wei, *in Proceedings of the 20th ICFA Advanced Beam Dynamics Workshop on High Intensity and High Brightness Hadron Beams*, Fermilab, 2002 (AIP, Melville, NY, 2002); J.A. Holmes, S. Cousineau, V.V. Danilov, S. Henderson, A. Shishlo, Y. Sato, W. Chou, L. Michelotti, and F. Ostiguy, *in The ICFA Beam Dynamics Newsletter*, Vol. 30, 2003.

[5] H. Grote and F.C. Iselin, "The MAD Program Version 8.19 User's Reference Manual", CERN/SL/90-13 (AP) (Rev. 5) (1996), CERN; F.C. Iselin, "The MAD Program Version 8.19 Physics Methods Manual", CERN/SL/92 (AP) (1994), CERN.

[6] D.A. Bartkoski, A.V. Aleksandrov, S.M. Cousineau, S. Henderson, and J.A. Holmes, *in Proceedings of the European Particle Accelerator Conference (EPAC06)*, Edinburgh, Scotland, 2006.

[7] J.A. Holmes, S.C. Bunch, S.M. Cousineau, V.V. Danilov, S. Henderson, A.P. Shishlo, Y. Sato , and M. Plum, *in Proceedings of the European Particle Accelerator Conference (EPAC04)*, Lucerne, Switzerland, 2004.

[8] J. A. Holmes, V. V. Danilov, and L. Jain, *in Proceedings of the 2005 Particle Accelerator Conference*, Knoxville TN, May 2005.

[9] A. Chao, "Physics of Collective Beam Instabilities in High Energy Accelerators", John Wiley and Sons, (New York), 1993.

[10] V.V. Danilov and J. Holmes, *in Proceedings of Halo '03, ICFA Advanced Beam Dynamics Workshop*, (Montauk NY), May, 2003.

[11] H. Hahn, Brookhaven National Laboratory, *private communication*, 2004.

[12] R. Macek, et al, *in Proceedings of the 2005 Particle Accelerator Conference*, Chicago, June 2001, p. 688.

[13] A. P. Shishlo, S. M. Cousineau, V. V. Danilov, S. Henderson, J. A. Holmes, and M. A. Plum, *in Proceedings of the European Particle Accelerator Conference (EPAC06)*, Edinburgh, Scotland, 2006.

[14] M.A. Furman and M.T.F. Pivi, Phys. Rev. ST Accel. Beams 5, 124404 (2002).

[15] V. V. Danilov, A. V. Aleksandrov, S. Assadi, W. Blokland, S. M. Cousineau, C. Deibele, S. Henderson, J. A. Holmes, M. Plum, and A. P. Shishlo., *in Proceedings of the 39th ICFA Advanced Beam Dynamics Workshop on High Intensity and High Brightness Hadron Beams*, Tsukuba, Japan, 2006.